Agricultural and Forest Meteorology 259 (2018) 211–221

Contents lists available at ScienceDirect

Agricultural and Forest Meteorology

journal homepage: www.elsevier.com/locate/agrformet

Forest productivity varies with soil moisture more than temperature in a small montane watershed

Liang Wei[a,b,1], Hang Zhou[c,d,1], Timothy E. Link[b], Kathleen L. Kavanagh[e], Jason A. Hubbart[f], Enhao Du[b], Andrew T. Hudak[g], John D. Marshall[b,h,*]

[a] Los Alamos National Laboratory, Earth and Environmental Sciences Division, MS: J495, Los Alamos, NM 87545, USA
[b] Department of Forest, Rangeland, and Fire Sciences, University of Idaho, Moscow, ID, 83844, USA
[c] Descartes Labs, Inc, 1613 Paseo De Peralta Ste. 200, Santa Fe, NM, 8750, USA
[d] Department of Geography, University of Idaho, Moscow, ID, 83844, USA
[e] Department of Ecosystem Science and Management, Texas A&M University, 305 Horticulture and Forest Science Building, MS 2138, College Station, TX, 77843-2138, USA
[f] West Virginia University, Institute of Water Security and Science, Davis College, Schools of Agriculture and Food, and Natural Resources. 1098 Agricultural Sciences Building, Morgantown, WV, 26506, USA
[g] Rocky Mountain Research Station, United States Forest Service, Moscow, ID, 83843, USA
[h] Department of Forest Ecology and Management, Swedish Agricultural University, Skogmarksgränd, Umeå, 90736, Sweden

ARTICLE INFO

Keywords:
Cold-air drainage
Soil moisture
Environmental lapse rate
Tree height
$\delta^{13}C$
Forest growth

ABSTRACT

Mountainous terrain creates variability in microclimate, including nocturnal cold air drainage and resultant temperature inversions. Driven by the elevational temperature gradient, vapor pressure deficit (VPD) also varies with elevation. Soil depth and moisture availability often increase from ridgetop to valley bottom. These variations complicate predictions of forest productivity and other biological responses. We analyzed spatiotemporal air temperature (T) and VPD variations in a forested, 27-km^2 catchment that varied from 1000 to 1650 m in elevation. Temperature inversions occurred on 76% of mornings in the growing season. The inversion had a clear upper boundary at midslope (~1370 m a.s.l.). Vapor pressure was relatively constant across elevations, therefore VPD was mainly controlled by T in the watershed. We assessed the impact of microclimate and soil moisture on tree height, forest productivity, and carbon stable isotopes ($\delta^{13}C$) using a physiological forest growth model (3-PG). Simulated productivity and tree height were tested against observations derived from lidar data. The effects on photosynthetic gas-exchange of dramatic elevational variations in T and VPD largely cancelled as higher temperature (increasing productivity) accompanies higher VPD (reducing productivity). Although it was not measured, the simulations suggested that realistic elevational variations in soil moisture predicted the observed decline in productivity with elevation. Therefore, in this watershed, the model parameterization should have emphasized soil moisture rather than precise descriptions of temperature inversions.

1. Introduction

In the western US, 70% of the terrestrial carbon sink is located above 750 m elevation, 50%–85% of which is hilly or mountainous (Schimel et al., 2002). However, it is more challenging to simulate ecosystem productivity in mountainous than in flat areas because climatic variables can vary dramatically over short distances in complex terrain (Barry, 1992; Holden et al., 2011b; Hubbart et al., 2007a) and the eddy-covariance technique, which is often used for model parameterization, is difficult to use in complex terrain (Novick et al., 2014; Yi, 2008).

Fine-scale microclimate heterogeneity in mountainous areas can be observed in many variables including precipitation, shortwave radiation (0.28–3.5 μm), and air temperature (*T*). For example, precipitation typically increases with elevation (Barry, 1992; Kräuchi et al., 2000). Shortwave radiation varies between aspects and slopes and may be blocked by surrounding topography (Duursma et al., 2003). Similarly, air temperature is related to topographic features, especially aspect and elevation (Ashcroft and Gollan, 2012; Holden et al., 2011a; Holden et al., 2011b; Hubbart et al., 2007a; Suggitt et al., 2011) and topographic position (Daly et al., 2010). Temperature generally decreases with increasing elevation. However, due to nocturnal longwave

* Corresponding author at: Department of Forest Ecology and Management, Swedish Agricultural University, Skogmarksgränd, Umeå, 90736, Sweden.
E-mail address: john.marshall@slu.se (J.D. Marshall).
[1] Authors contributed equally to this work.

https://doi.org/10.1016/j.agrformet.2018.05.012
Received 20 November 2017; Received in revised form 7 May 2018; Accepted 11 May 2018

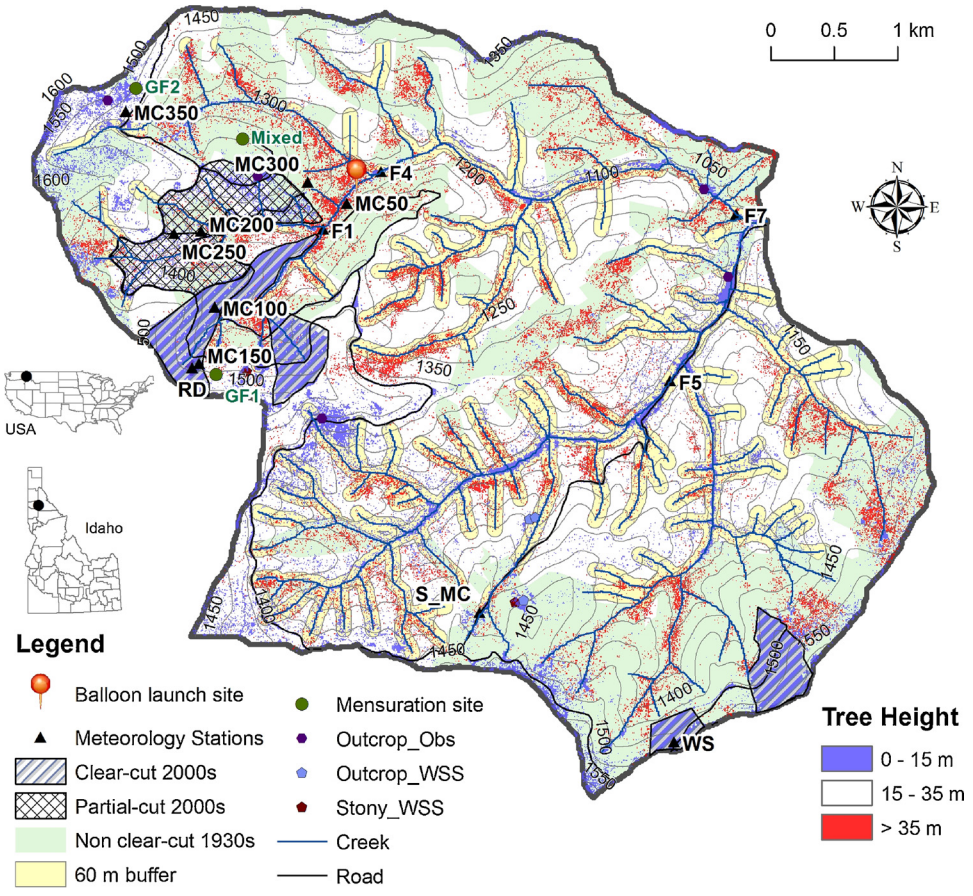

Fig. 1. Map of Mica Creek Experimental Watershed (MCEW). Elevation decreases from the southwest (1600 m) to the northeast (1000 m). Fifteen hydrometeorological stations were installed throughout the watershed (F2 station is located within 20 m of F1; not marked). Most of the area was clearcut around 1930 ("1930s-clearcut area"), but some area was not clear cut ("non-clear-cut area"). Lidar-derived vegetation height (collected in 2003) demonstrated that tall trees often occurred in the non-clear-cut area and near the creek ("60 m buffer" area). Short vegetation was common at the high elevation, which may be related to stony soil. Stony areas and outcrops are marked on the map; these were obtained either from the Web Soil Survey (WSS, Natural Resource Conservation Service, http://websoilsurvey.nrcs.usda.gov) or our field observations (Obs). Thin gray lines are contour lines (meters above sea level). Helium-filled balloons were launched from a ~one-hectare clearing between the MC50 and F4 station.

radiation emission, cold, dense air may produce katabatic flows that drain to valley bottoms, thereby reversing the temperature lapse rate and producing temperature inversions (Fleagle, 1950a; Fleagle, 1950b; Whiteman, 2000). The pool of cold air usually dissipates after shortwave radiation warms the ground, but the dissipation process may take up to five hours after sunrise (Manins and Sawford, 1979).

Inversions complicate the prediction of climate patterns in mountainous areas. Regional-scale weather conditions may not be sufficient to predict air temperature, especially in valleys (Bigg et al., 2014; Daly et al., 2010; Holden et al., 2011a; Lundquist et al., 2008) and the average environmental lapse rate (-0.0065 $^{\circ}$C m^{-1}) may not be a reliable predictor of air temperatures (Minder et al., 2010).

Due to the elevational heterogeneity of microclimate variables, plants at different elevational positions may differ in their growth responses, especially when they are under stress (Elliott et al., 2015). Therefore, it would be challenging to predict forest productivity in mountainous areas. The topographic effects on radiation intensity and terrain shading (i.e., the hillshade effect) reduce solar radiation in the valley, which may either reduce forest productivity if the tree growth is radiation limited, or increase productivity if trees are under water stress. Warm temperature generally benefits photosynthesis and productivity (Way and Oren, 2010). However, higher temperature also accompanies higher vapor pressure deficit (VPD); both high temperature and high VPD increase evapotranspiration and hence increase plant water stress. High VPD also leads to stomatal closure, which limits photosynthesis. Therefore, the benefit of higher temperature on photosynthesis may be diminished by higher VPD.

Nocturnal temperature inversions may reverse the usual temperature gradient, which may impact forest productivity in mountainous areas. Low temperatures on inversion days reduce respiration in the valley (Novick et al., 2016), but restrict photosynthesis if inversions persist in the daytime. Inversions may also reduce the growing season length (Adams, 1979), which further reduces forest productivity. As regional warming proceeds, cold air drainage may cause microclimate to further deviate from regional climate (Daly et al., 2010; Keppel et al., 2012), which will further increase the difficulties of predicting temperature effects on forest productivity. It is hence an urgent need to accurately estimate microclimate in mountainous areas with cold-air drainage and to model its impact on forest productivity.

Besides microclimate variables, soil depth and hence available soil moisture can vary considerably over short distances in mountainous areas. Although low elevation typically have lower precipitation than high elevation (Barry, 1992; Kräuchi et al., 2000), soil depth and moisture availability often increase from ridgetop to valley bottom (Bolstad et al., 2001; Helvey et al., 1972; Lin et al., 2006; Markesteijn et al., 2010; Yeakley et al., 1998). This is because topography modifies water flow and particle redistribution, topographic characteristics like slope and flow accumulation determine soil properties (Gessler et al., 2000; Gessler et al., 1995; Moore et al., 1993). Therefore, forest productivity in the valley normally benefits from deep soil and extra soil moisture, while productivity on ridges may suffer more from drought due to shallower soil than in the valley (Bolstad et al., 2001). Note that air temperature also generally increases from ridgetop to valley bottom in the absence of inversions, which makes it difficult to separate the impact of air temperature and soil moisture on forest productivity; inversions may break the confounding of these variables.

The general objective of this study was to assess the respective influences of microclimate and soil moisture on forest ecosystem processes on a small forested watershed in complex terrain. Specific objectives were three-fold. First, we aimed to understand the spatiotemporal dynamics of temperature inversions in a small forested catchment. Second, we used 3-PG, a quasi-mechanistic forest growth model, to analyze the effects of inversions and soil depth on forest productivity. Thirdly, we ran models of different scenarios to determine

which of the climatic or soil factors is most important to determine elevational trends of forest productivity.

2. Methods

2.1. Study area

The study catchment, Mica Creek Experimental Watershed (MCEW), is located in northern Idaho, USA (MCEW; 47°10′N, 116°16′W) (Fig. 1). MCEW is dominated by a forest of grand fir (*Abies grandis* (Douglas ex D. Don) Lindl.), western redcedar (*Thuja plicata* Donn ex D. Don), Douglas-fir (*Pseudotsuga menziesii* (Mirb.) Franco), and western larch (*Larix occidentalis* Nutt.) (Fig. S4). Soils were formed in volcanic ash deposits of varying depth over loess and weathered bedrock, which was mostly metaphorphosed gneiss and quartzite (Hubbart et al., 2007a). Soils belong mostly to the Bouldercreek-Marblecreek association (49%), Bouldercreek ashy loam (41%), and Marblecreek-Rock outcrop complex (4%) (web soil survey (WSS) of USDA Natural Resources Conservation Service, 2011; http://websoilsurvey.nrcs.usda.gov). Most of the area was clearcut around 1930 (Fig. 1 and S3). It was free of major anthropogenic disturbances from ~1930 to 2001, when experimental clear- and partial-cut (50% canopy removal) harvests were completed. (Fig. 1).

The watershed is comprised of two headwater catchments, which combine to form the main stem of Mica Creek (Fig. 1). Elevation ranges from 1000 m (East) to 1650 m (West) (Fig. 1). The physiography of the MCEW lends itself to temperature inversions because the watershed is generally east-facing, in the lee of prevailing winds, and steeply sloped, thereby shading valley bottoms (Hubbart et al., 2007a). The watershed was not glaciated, which has resulted in V-shaped valleys with deep dissection and narrow flow paths in the valley bottoms. A detailed description of MCEW can be found in Hubbart et al. (2007a, b).

2.2. Automated meteorological data

MCEW was instrumented with 15 meteorological stations spanning an elevation range from 1008 to 1469 m (Table 1, Fig. 1). These stations were originally established for a suite of hydrological and ecological studies (Du et al., 2014; Du et al., 2016; Hubbart et al., 2015; Hubbart et al., 2007b; Wei et al., 2014a) and located specifically to capture major hydrometeorological variations within the watershed. Meteorological observations included air temperature (°C, observed at 14 stations; but one was excluded, see below), precipitation (mm, 7 stations), vapor pressure (e_a, kPa, 10 stations), and shortwave and longwave radiation (W m^{-2}, 1 station) (Table 1). All temperature/humidity probes were installed in standard Gill multi-plate shields to reduce radiation-induced errors. Even when shielded, temperature errors have been noted to occur, but are typically much less than 0.9 °C during daytime hours and < 0.1 °C during nocturnal conditions (Nakamura and Mahrt, 2005); for this study, temperature corrections were not applied, since most meteorological stations were located in well-ventilated and/or shaded locations.

Four long-term stations were outfitted with hydrometeorological equipment in the early 1990s at selected Flume Stations "F": (F1, F4, F5, and F7). Two additional long-term hydrometeorological stations were established in the mid-1990s (RidgeSnow, "RD"; WindSolar, "WS"). Measurements included: air temperature and relative humidity (RH; added in the mid-1990s) at F1 and F7 (Vaisala HMP45C, Campbell Scientific, Logan, UT) and air temperature at F4 and F5 (CS107, Campbell Scientific, Logan, UT), where all were installed approximately 3 m above ground. At RD and WS, we measured air temperature, wind speed or wind speed and direction (cup anemometer Model 014 A or cup anemometer Model 034B, Met One Instruments, Grants Pass, OR, USA), and shortwave radiation (LI-200 pyranometer, LI-COR Corporation, Lincoln, Nebraska; ~7 m above ground) (Table 1). The WS site was upgraded in 2004 with the addition of a temperature/humidity sensor (HMP45C) and a longwave radiation sensor (CG-1, Kipp& Zonen Inc., Delft, the Netherlands). The Mica Creek Snow Telemetry, (SNOTEL) Natural Resources Conservation Service, site number 623, "S_MC" provided total precipitation, snow water equivalent, snow depth, and air temperature data beginning in 1991. However, air temperature data from this site were affected by biases that reported spuriously amplified warming trends in the region (Oyler et al., 2015 and Phil Morrisey, personal communication); we hence excluded the temperature data from this site. Finally, seven hydrometeorological stations (MC50 – MC350, Table 1) recorded data from October 2003 and to April 2007. Measurements and sensors were the same as at the long-term stations; detailed descriptions of these stations can be found in Du et al. (2016), Hubbart et al. (2007a), and Hubbart et al. (2015). For the seven MC hydrometeorological stations, all temperature, humidity, and wind sensors were installed approximately 2 m above ground. Because 2005 and 2006 had the most complete meteorological

Table 1
Information describing the meteorological stations in MCEW for the 2005 and 2006 records, sorted by elevation. Slopes and aspects were obtained from a digital elevation map. Stations beginning with "F" are Flume stations; those beginning with "MC" are short-term meteorological stations. The SNOTEL station at Mica Creek is abbreviated to S_MC, RidgeSnow to RD, and WindSolar to WS. Acronyms: T = air temperature, H = relative humidity, P = precipitation, W = wind, and R = solar radiation.

	Station ID.	Elevation (m)	Slope (°)	Aspect (°)	Duration	Available items	Time Step (min)	Location
1	F7	1008	11	82	Since Jan. 1992	T, P	30	Creek side/Under canopy
2	F5	1054	3	142	Since Oct. 1992	T, P	30	Creek side/Under canopy
3	F4	1172	4	49	Since Oct. 1992	T, P	30	Creek side/Under canopy
4	MC50	1192	15	307	Aug. 2004- Jan. 2007	T, H, W	30	Creek side/Under canopy
5	F1	1205	6	319	Since Jan. 1992	T, H, P	30	Creek side/Under canopy
6	F2	1205	0	–	Since Oct. 1998	P	30	Creek side/Under canopy
7	MC300	1299	14	96	Nov. 2003 - Dec. 2006	T, H, W	30	Under canopy
8	MC200[a]	1327	16	70	Nov. 2003 - May 2007	T, H, W	30	Under canopy
9	MC100[a]	1359	20	80	Nov. 2003 - May 2007	T, H, W	30	Clearcut
10	S_MC[a,b]	1375	6	106	Since Oct. 1990	P	60 or 180[c]	Forest gap
11	MC250	1388	15	103	Aug. 2004- Dec. 2006	T, H, W	30	Under canopy
12	MC150	1431	16	358	Aug. 2004- May 2007	T, H, W	30	Clearcut
13	RD[a]	1442	20	10.2	Since Nov. 1996	T, P	30	Clearcut
14	MC350	1463	25	153	Aug. 2004- May 2007	T, H	30	Under canopy
15	WS[a]	1469	0	–	Nov. 1997- Apr. 2008	T, H, W, R	15	Clearcut

[a] stations in clearcut or gap in thinned forest.
[b] Temperature data of S_MC were available but not used due to biases of the temperature sensor (see Methods).
[c] 180 min time step in 1/8 -2/16/2006.

data among all available years (Table 1), we analyzed the data from these two years.

The aspect and slope for the stations varied and some stations were located under canopy and some were in clear-cut areas (Table 1). The canopy did not appear to have a marked impact on the elevational differences in air temperature (see Discussion), so we used data from all stations to describe the temperature lapse rates. We have marked stations in clearcuts or gaps with "*" in the figures to differentiate them from stations under the unharvested forest canopies.

We used potential temperatures to estimate the inversions and used observed temperature (dry-bulb temperature) for forest growth modeling. The potential temperatures represent the temperature an air parcel would attain if it were brought to sea level (Wallace and Hobbs, 2006). Using potential temperatures removes the impact of the elevational pressure gradient on the temperature and hence allows direct comparisons of temperature measurement across elevations. Moreover, it describes the potential for cold-air drainage during radiation cooling insofar as a decrease in potential temperature with decreasing elevation suggests that an air parcel may flow downward despite warming induced by the rise in pressure with decreasing elevation.

2.3. Mid-valley atmospheric profiling

We attached 13 radiation-shielded air temperature sensors (Hubbart et al., 2005) (Thermochron iButton, Maxim Integrated Products, Inc., Sunnyvale, CA, USA) to two helium-filled tethered balloons of two meters diameter. The balloons provided sufficient lift to carry the rope and sensors to 206 m above the valley bottom. The influence of radiation on the temperature measurements were reduced with the shields, which were subsequently found to be biased from +1.8 to + 3.0 °C during the day under naturally-ventilated conditions in forested and open areas, respectively and negligible during nocturnal conditions (Terando et al., 2017). The balloons were launched from a ~one-hectare clearing between the MC50 and F4 station (Fig. 1). The launch occurred once winds subsided around 16:00 on July 24, and the balloon was retrieved as winds resumed around 10:00 on July 25, 2006. The launch site was ~1200 m a.s.l. and the forest canopy adjacent to the clearing was approximately 35 m in height. Air temperatures were recorded every 10 min from 20:30 to 9:00 the next day at 1, 6, 14, 26, 46, 77, 86, 106, 126, 146, 166, 186 and 206 m above ground level.

2.4. Forest growth model simulations

Dramatic elevation differences in air temperature and VPD might impact the productivity and water use of the forest. We used a semi-mechanistic model, 3-PG (Physiological Principles Predicting Growth, Landsberg and Waring, 1997), to test these potential effects (see Notes S1 for model descriptions). We chose 3-PG because it is sensitive to climate variables; it has been successfully applied to test the effect of climate variables on forest growth at the stand and regional scales (Almeida et al., 2010; Coops and Waring, 2011; Coops and Waring, 2001). The effect of temperature on forest growth was estimated as a temperature modifier (f_T) and a frost modifier that reduces photosynthesis from its thermal optimum (modifier value from 0 to 1; see supplementary material) (Landsberg and Waring, 1997). When temperature is higher or lower than the species-specific optimum, the value of f_T decreases. The frost modifier completely removes photosynthesis after a frosty night (Eqn A4 in supplementary material). The effect of VPD was estimated as the decreasing canopy conductance and photosynthesis with increasing VPD (Landsberg and Waring, 1997) (see supplementary material). This model was also shown to be useful in simulating the impact of soil moisture on forest growth (Almeida et al., 2010; Wei et al., 2014a; Wei et al., 2014b).

The 3-PG model was previously parameterized at MCEW based on a suite of field measurements including transpiration, stem mass, basal area, leaf area index, and stocking from a former study (Wei et al., 2014a) (see Notes S2 "Forest Measurement"). The model was extended to estimate tree-ring stable isotopes ($\delta^{13}C$) in Wei et al. (2014a) and Wei et al. (2014b) (see Notes S1); the $\delta^{13}C$ values reflect the intrinsic water use efficiency of forests (Farquhar et al., 1989). The simulation of annual tree ring $\delta^{13}C$ and transpiration also reasonably fit the measurements, which provided an independent test of the model structure and the quality of the parameter set for MCEW (Wei et al., 2014a). Reasonable simulations of $\delta^{13}C$ also validated the simulations of gross primary production (GPP) and canopy conductance, as the simulations of $\delta^{13}C$ were calculated from GPP and canopy conductance (Wei et al., 2014a). We hence used the parameter values from site GF1 (Fig. 1) in Wei et al. (2014a) to drive the model.

The only new measurement beyond Wei et al. (2014a) was quantum yield, which we use to estimate the light-use efficiency of photosynthesis. Using the techniques of Nippert and Marshall (2003), we measured quantum yield for grand fir at the top and bottom of the canopy for 29 trees at five sites in MCEW (Wei et al., 2008; Wei et al., 2014a). There were no significant differences between canopy position or among sites ($\alpha = 0.05$). The mean value was 0.057 (0.0033 SE; mol CO_2 mol^{-1} photon), which we used throughout this study.

We simulated the forests as even-aged and compared the simulations with observed tree heights. We made two major simplifications to isolate the climatic factors and soil moisture in our simulations. First, the forest over nearly the entire catchment was regenerated from clear-cutting around 1930 and was therefore even-aged; we delineated the clear-cut areas based on aerial photos of 1933 and only use such areas for model validation (see section 2.5). Second, we used grand fir as our "model species" and modeled the watershed as if the canopy were 100% grand fir; we thus ignored the variation in species composition and used parameters for grand fir for every grid cell in MCEW. Grand fir is the dominant species in MCEW, comprising 48% of the tree stems on the site. Grand fir is also similar in its ecophysiological characteristics to the other dominant species on the watershed (Duursma et al., 2007; Duursma et al., 2003). Because dissimilar species may respond to hydroclimatic factors very differently in the same habitat (Elliott et al., 2015; Galmés et al., 2007; Johnson et al., 2018), the dominance of grand fir and its similarity to co-occurring species in MCEW greatly simplified simulations.

Although 3-PG cannot capture the possible impact of cold air specifically on autotrophic respiration (R_a) during the night (e.g. Novick et al., 2016), we argue that it is a suitable tool for simulating long-term forest productivity in this study. It assumes a constant NPP/GPP ratio, or carbon-use efficiency (CUE). A fixed CUE has been supported by observations at annual or longer temporal scale for natural forests (Campioli et al., 2015; Litton et al., 2007; Malhi et al., 2017; Vicca et al., 2012; Waring et al., 1998), albeit with some exceptions (DeLucia et al., 2007; Goulden et al., 2011). More importantly, studies also show that the CUE does not change with stand age (Campioli et al., 2015; Litton et al., 2007; Vicca et al., 2012), and was not sensitive to climatic drivers (Campioli et al., 2015; Litton et al., 2007; Malhi et al., 2017; Vicca et al., 2012). Most important of all, CUE did not change with elevation in mountain valleys of Peru (Malhi et al., 2017). Even in the humid tropics, nighttime inversions may be present (Goulden et al., 2006), so the constancy of CUE argues that 3-PG can be relied upon here as well, at least for this first attempt at modeling inversion effects.

We translated the 3-PG model to the Python programming language (http://www.python.org/) and ran it over the MCEW on 30-m grids (n = 30011). Meteorological data (temperatures, VPD, and solar radiation) were interpolated for each 30-m grid to drive the model (see Notes S6). We used lapse rates of two elevational bands (inside or outside temperature inversions; see Results for detail) estimated from the 13 stations (Table 1) to interpolate half-hourly temperature for all grid cells; we then estimated monthly mean daily minimum (T_{min}) and maximum temperature (T_{max}) for all grid cells and used these values to drive the model. VPD was estimated with e_a and interpolated temperature for each grid cell (see Notes S6). Spatiotemporal distribution of

shortwave radiation also accounted for the effects of topographic shading and cloud cover (Note S6 and Fig. S1). Precipitation data from the S_MC station were used across the watershed as there was no difference in precipitation across elevations based on observations from seven stations (see Notes S6 and Fig. S13). We repeatedly concatenated meteorological data from these two years to create a 77-year time series to drive the model from 1930 to 2006 for each grid.

We simulated the impacts of microclimatic factors on GPP, tree height, tree ring $\delta^{13}C$, and transpiration, which is related to photosynthetic water-use efficiency. We first ran 3-PG with interpolated T, VPD, and solar radiation that was spatially variable, but with identical maximum available soil water (ASW_x, synonym as maximum available water-holding capacity; set at 150 mm) across elevations as the reference scenario (noted "Reference"). This scenario represented combined elevational effects of T, VPD, and solar radiation on forest productivity.

We also ran the model to estimate the impact of the hillshade effect on forest productivity (noted "No Hillshade"). The hillshade effect (Fig. S1 and Note S6) was neglected in estimates of solar radiation in this scenario. The hillshade effect reduced solar radiation especially in the valley by as much as 33% (Fig. S1).

We ran the model in the third scenario (denoted "Soil Moisture") to estimate the impacts of soil moisture on forest growth dynamics. Both soil depth and water content, and hence ASW_x, may vary significantly with slope and aspect; soil moisture has been shown to decline from the valley floor to ridgetop (Bolstad et al., 2001; Helvey et al., 1972; Yeakley et al., 1998). Differences in ASW_x varied from 80 mm to 150 mm within MCEW based on the Web Soil Survey (WSS, http://websoilsurvey.sc.egov.usda.gov) and from 80 mm to 300 mm based on observations (e.g. Fig. S6). Therefore, ASW_x was set to decrease linearly from 300 to 80 mm with increasing elevation in the Soil Moisture scenario. The varied ASW_x was intended to capture the general trend of increased soil depth and moisture from ridge to valley (Bolstad et al., 2001; Helvey et al., 1972; Lin et al., 2006; Markesteijn et al., 2010; Yeakley et al., 1998). We were forced to make this simple assumption about ASW_x because a detailed description of ASW_x was lacking.

2.5. Tree height

We used tree height measured from airborne lidar (light detection and ranging) as an indicator of cumulative forest productivity for the even-aged stands in MCEW (Fig. 1). The airborne lidar data were collected in 2003 using a Leica ALS40 lidar system (Hudak et al., 2006; Hudak et al., 2008; Jensen et al., 2008). The data were collected at a pulse density of 1–2 m^{-2}, from which a maximum height raster grid was generated at a 6 m resolution. We upscaled the maximum height to 30 m resolution to match the resolutions of our 3-PG simulations. We used the lidar-based tree heights as the indicator of forest productivity and compared them with modeled tree height. Although tree height was not simulated in the original 3-PG, we estimated it with a diameter-based model (Wykoff et al., 1982) (Fig. S5) that converted modeled stem mass into height.

This study is a novel example of using maximum tree height to compare with model results. In an earlier study, tree height was moderately related to 3-PG simulated GPP and MODIS estimated GPP (Spearman's rank correlation = 0.65 and 0.70 respectively) across 11 US western states, including Idaho (Weiskittel et al., 2011). The use of tree height requires that age and species are known and they have grown in an even-age cohort (Weiskittel et al., 2011). Our study matches these requirements. First, most area in the watershed was in even-aged forests regenerated after clearcutting in the 1930s (Fig. S3) and we were also able to delineate the clearcut area using aerial photos from 1933 (see next paragraph). Second, grand fir was the tallest tree species at stand age ~75 years (Fig. S4) when the lidar data were collected. Therefore, we compared the observed maximum tree heights in each 30 m grid (see Section 2.5) to simulated tree heights across the watershed.

We used aerial photos from 1933 to delineate the even-aged forests that had been clear-cut in the 1930s (Fig. S3). We call this area the "1930s-clearcut area" (Fig. 1). Trees regenerated from seed after the 1930s-clearcut areas, with no major human or natural disturbances since the 1930s except for road construction in 1997 and logging of small patches of forest in 2000 (Fig. 1). Because trees around the creek were less likely to encounter drought than other areas (e.g. Fig. S6), and large old growth trees (primarily cedars) were not cut in some riparian areas, we partitioned the 1930s-clearcut area into the area within 60 m of creeks ("Riparian area") and the rest of 1930s-clearcut area ("Main area"). By analyzing the lidar-derived 2-m digital terrain model (DTM), we found that the slopes adjacent to creeks are generally steeper than those farther from the creeks; thus, areas within 60 m distance from the creeks served as an efficient natural divide, accounting for ~80% of areas with slopes > 30°. We then estimated the change in tree height with elevation in both the Riparian and Main areas.

3. Results

3.1. Boundary of cold-air pool

Based on data from the tethered balloon (Fig. 2) and the meteorological stations (Fig. 3), we located a consistent upper boundary of the cold-air pool at ~1370 m during nights with temperature inversions. This level is approximately 170 m above the valley floor; the cold air pool thus covered approximately 85% of the MCEW area (Fig. S2). The specific boundary and area of the cold air pool may be affected by small biases in temperature measurements due to radiative heating, although the general pattern was very distinct based solely the under-canopy stations with the lowest potential biases. We therefore separated the watershed into three elevation classes: low (1000 – 1359 m), medium (1359–1388 m), and high (1388 – 1650 m) (also see Notes S3 for more detail).

3.2. Frequency and strength

The temperature inversions occurred year-round, however, they were most frequent during the growing season, from May-October (Fig. 4). We estimated the lapse rate for low and high elevations at

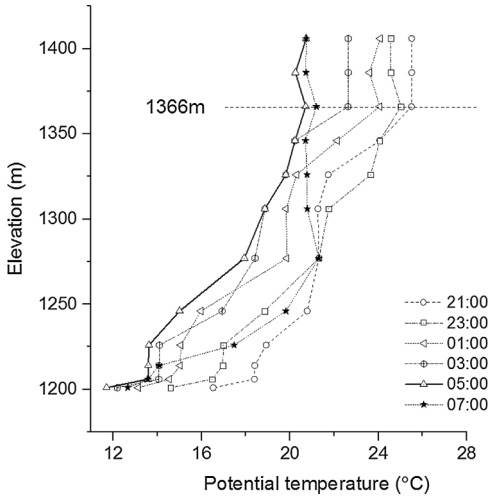

Fig. 2. A 10-hour profile (July 24–25, 2006) of potential temperature exhibiting a temperature inversion in the MCEW. Temperature sensors were tethered on a rope under a helium balloon and distributed at different heights above the ground (1, 6, 14, 26, 46, 77, 86, 106, 126, 146, 166, 186 and 206 m). The ground elevation was ~1200 m and the boundary of the cold air pool was at ~1366 m a.s.l. during nighttime. Open symbols indicate nighttime measurements from sunset (20:29) to sunrise (05:15).

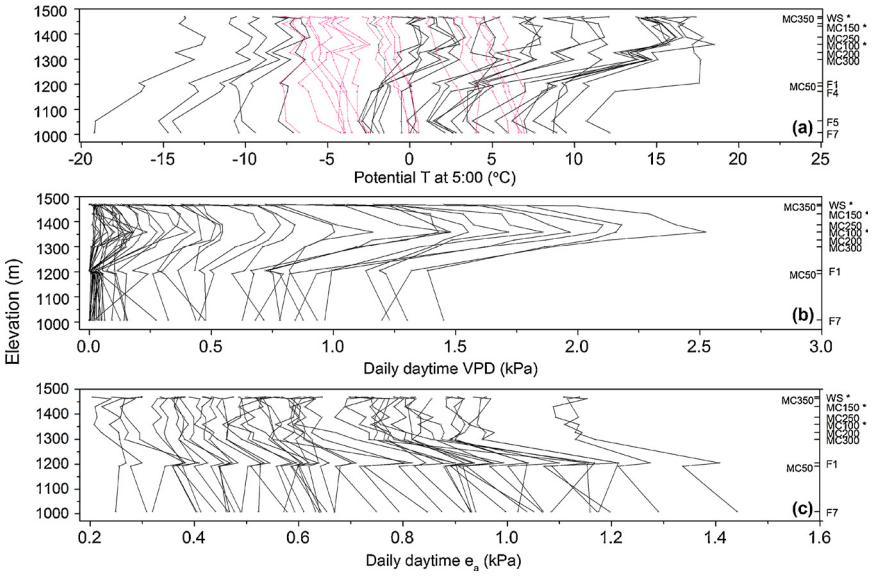

Fig. 3. The potential temperature at 05:00, mean daytime VPD, and mean daytime water vapor pressure (e_a) in the MCEW. We present here just the 1st and 15th day in every month of 2005 and 2006 to limit the data clutter. (a) Inversions occurred in 30 out of 48 days (solid lines) and did not occur on the other 18 days (red dashed lines). On inversion days, potential air temperature increased with elevation below either 1359 m (MC100) or 1388 m (MC250); it decreased with elevation above 1388 m. (b) On most days, mean daytime VPD was low at the three riparian sites. Mean daytime VPD peaked at either 1359 m or 1388 m on most days. (c) The three riparian sites (F7, MC50, and F1) generally had higher e_a than sites at higher elevation. Stations marked with "*" were located in either clearcut or forest gaps; stations without "*" were located under canopy. (For interpretation of the references to colour in this figure legend, the reader is referred to the web version of this article).

05:00, the approximate time of the daily temperature minimum, for all days in both years. The lapse rate was estimated as the slope of the linear regression of elevation versus potential temperature; only significant regressions ($P < 0.05$) are shown (Fig. 4). If we define temperature inversion days as those with a significant positive lapse rate at 05:00, then temperature inversions occurred on 243 and 218 days in 2005 and 2006, respectively (Fig. 4a). During the growing season (May-October), inversions occurred on 76% of the days and 89% of days during the three warmest months (July - September). The strength of the temperature inversion also varied between seasons. The average 05:00 lapse rates of days with inversion were generally more positive during the growing season (May-Oct; 0.021 ± 0.010SD °C m^{-1}) than in cooler months (Jan-April, and Nov-Dec; 0.014 ± 0.007 °C m^{-1}) (Fig. 4a).

As a consequence of strong and frequent inversions (Figs. 3 and 4) and the persistence of the cold air pool (see SI), the medium elevation (1359–1388 m) was the warmest position on the slope year-round in terms of the mean daily temperatures. As shown in the observed monthly mean daily temperature (T_{ave}) and monthly mean daily T_{min}, the medium elevation had higher monthly T_{ave} and T_{min} in all months except May (Fig. S9b). Similar patterns were seen in monthly mean daily T_{min} (Fig. S9c), but not monthly mean daily T_{max} (Fig. S9).

3.3. VPD and e_a

Water vapor pressure (e_a) was similar across all elevations except for the three stations closest to the stream (Fig. 3c). Average e_a of riparian stations was 0.13 kPa higher than at the non-riparian stations based on the daily daytime averages (Fig. 3c). We believe that evaporation from the creek may have increased e_a at these three stations, which should only affect the area immediately next to the creek. We therefore did not use these three stations for e_a estimation (see discussion in Note S5). Across all elevations, the daily daytime VPD peaked at either 1359 or 1388 m (Fig. 3b), which followed the temperature trends. The observed patterns were used to interpolate VPD across elevations to drive the 3-PG model over the whole watershed (Notes S6).

3.4. Lidar tree height

Maximum tree height (H_x) decreased with increasing elevation within the 1930s-clearcut area (Fig. 5). One might expect that the dramatic elevational variations in air temperature and VPD should drive dramatic elevational variation in forest productivity, but height (H_x) did not peak at the medium elevation, where peak T and VPD occurred, around 1359–1388 m. We attribute this mismatch to the opposing effects of temperature, which would increase productivity, and VPD, which would decrease it. The two did not cancel completely,

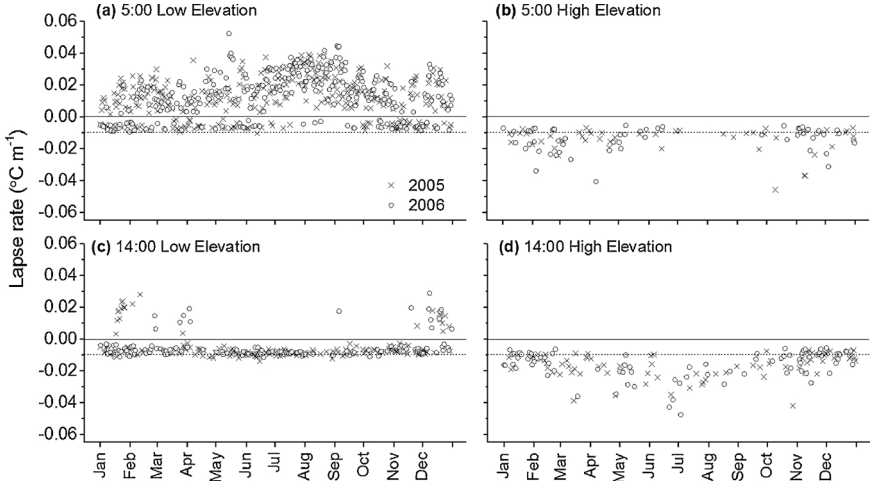

Fig. 4. Lapse rates of the potential temperature at 05:00 (approximate daily T_{min}) and 14:00 (approximate daily T_{max}) of each day in 2005 and 2006 in the MCEW. The lapse rate was estimated separately using eight meteorological stations at low elevation (1008 – 1359 m) and five stations at high elevation (1388–1469 m). Only the lapse rates with significant correlations are shown ($P < 0.05$). Positive lapse rates indicate inversions. Dotted lines show the dry-adiabatic lapse rate (-0.0098 °C m^{-1}). At low elevation, inversions occurred in most days at 05:00 (a), and the inversion persisted even at 14:00 in some winter days and one day in July 2006. Inversions did not occur at high elevation (b and d).

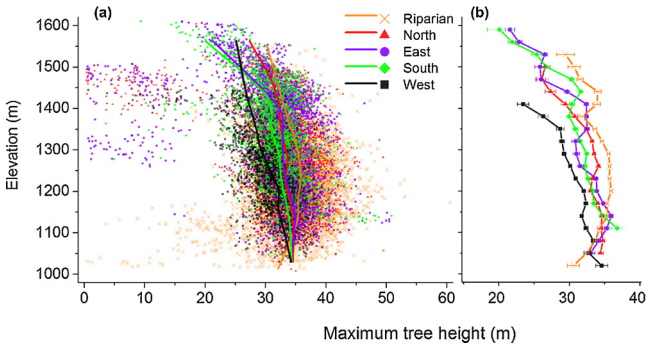

Fig. 5. Variations in tree height with elevation in the 1930s-clearcut area. (a) Each point represents the maximum tree height in a 30 × 30 m grid (H_x) from a lidar tree height map. The Riparian areas are 60 m buffer zones from creeks of 1st order and above within the 1930s-clearcut area, and four aspects in the Main area is the 1930s-clearcut area minus creek-area. We fitted H_x data using local polynomial regression (Cleveland et al., 1992) to show general elevational trends. (b) Tree heights were binned for each 30 m elevation band with n ≥ 10 grids. H_x decreased with increasing elevation in all four aspects of the Main area ($P < 0.05$) but not in the Riparian area. Error bars show standard errors.

resulted in a consistent upward trend. In riparian areas, H_x peaked at around 1200–1300 m (Fig. 5a). Not surprisingly, H_x in the riparian zone was greater than that in the Main area at all elevations above ~1100 m (Fig. 5). Trees were often > 35 m in height in Riparian areas (Fig. 1); in contrast, trees at the ridge top were sometimes less than 15 m in height (Fig. 1).

3.5. Modeling

Simulations with the three scenarios showed how T, VPD, hillshade, and ASW_x would impact the simulations of tree height, GPP, tree ring $\delta^{13}C$, and transpiration across elevations (Fig. 6). Data are shown from south-facing slopes of the Main area in year 2006 as the elevational trends were similar across all aspects. Despite dramatic elevational variation in T and VPD, simulated tree height and GPP in the Reference scenario varied little above ~1100 m in elevation. Removing hillshade (No Hillshade scenario) increased the solar radiation at low elevations, but the simulations of tree height, GPP, and transpiration increased only slightly. Applying decreasing ASW_x with increasing elevation (Soil Moisture scenario) increased tree height, GPP, and transpiration at elevations below ~1400 m but decreased them above ~1400 m relative to the Reference scenario. In terms of the elevational trends, simulated tree height and GPP in the Soil Moisture scenario were most similar to the observed H_x (Fig. 5b vs. Fig. 6a and b).

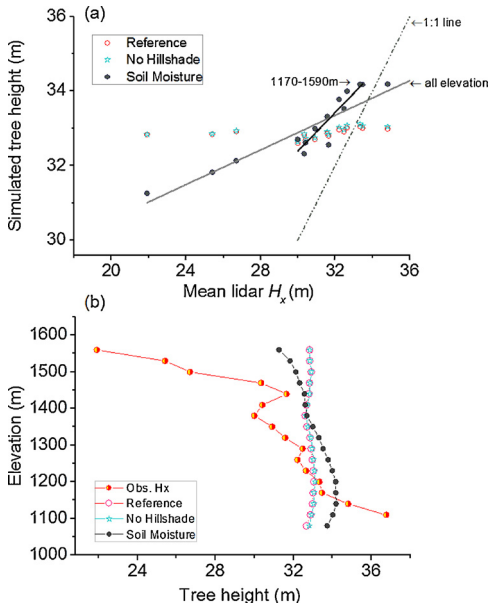

Fig. 7. Comparisons between simulated tree height and lidar observed maximum tree heights in 30 × 30 m grids (H_x). Data were binned for each 30 m elevation band. The three scenarios are the same as Fig. 6. Only the Soil Moisture scenario resulted in positive correlation with observed H_x at $\alpha = 0.05$ across all elevations (Fig a; grey solid line, $R^2 = 0.81$, $P < 0.001$). As shown in Fig b, observed H_x sharply decreased with increasing elevation above 1590 m likely due to rocky conditions; H_x was unrealistically high for 76-year old trees at the 1110–1140 m bin likely attributable to trees that were uncut near the creek in the 1930s (Fig. 5a). Removing those four data points at the highest and lowest elevations resulted in correlations between H_x and simulated tree height being significant at the 1170–1590 elevation band (black solid line, $R^2 = 0.81$, $P < 0.001$) and the regression line was closer to 1:1 line than that using data from all elevations.

We also compared simulated tree heights in 30 m elevational bands with lidar based tree heights H_x (Fig. 5b). Only simulations of the Soil Moisture scenario had positive linear correlations with lidar-based observations at $\alpha = 0.05$ among all three scenarios for all elevations and the 1170–1590 m band (both $R^2 = 0.81$, $P < 0.001$; see Fig. 7 for detail). This confirmed that the Soil Moisture scenario was the most realistic scenario for predicting tree height.

The simulations of tree ring $\delta^{13}C$ increased from ~-27.8 to ~-26.2‰ with increasing elevation in all scenarios (linear regressions,

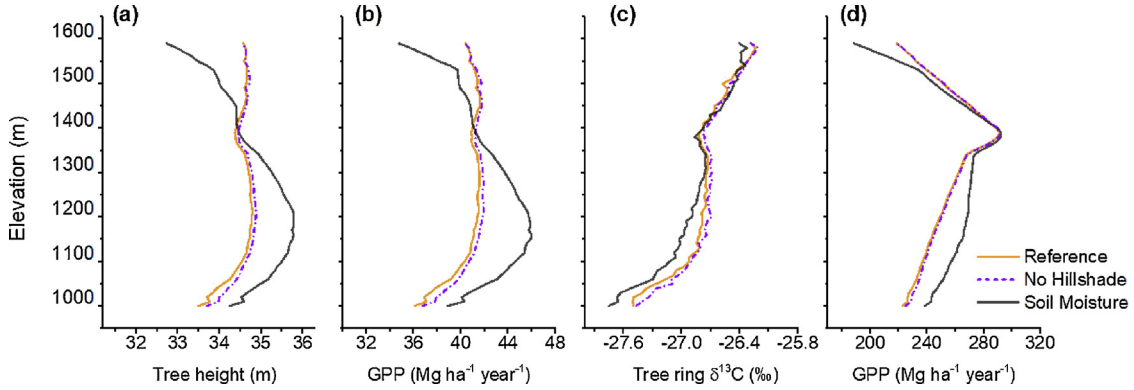

Fig. 6. We created three scenarios to separate the impacts of environmental factors on the simulations of tree height, GPP, $\delta^{13}C$, and transpiration. The three scenarios included: "Reference", testing the combined effect of climatic factors (T, VPD, and radiation) and all grids used identical ASW_x = 150 mm; "No Hillshade", hillshade was removed to test hillshade effect by comparing with the Reference; and "Soil Moisture", testing impact of soil moisture and ASW_x increased linearly from 80 to 300 mm with decreasing elevation, which is also the most realistic scenario. All three scenarios used the same dataset of interpolated T and VPD data. Data shown are simulations based on the south facing slope.

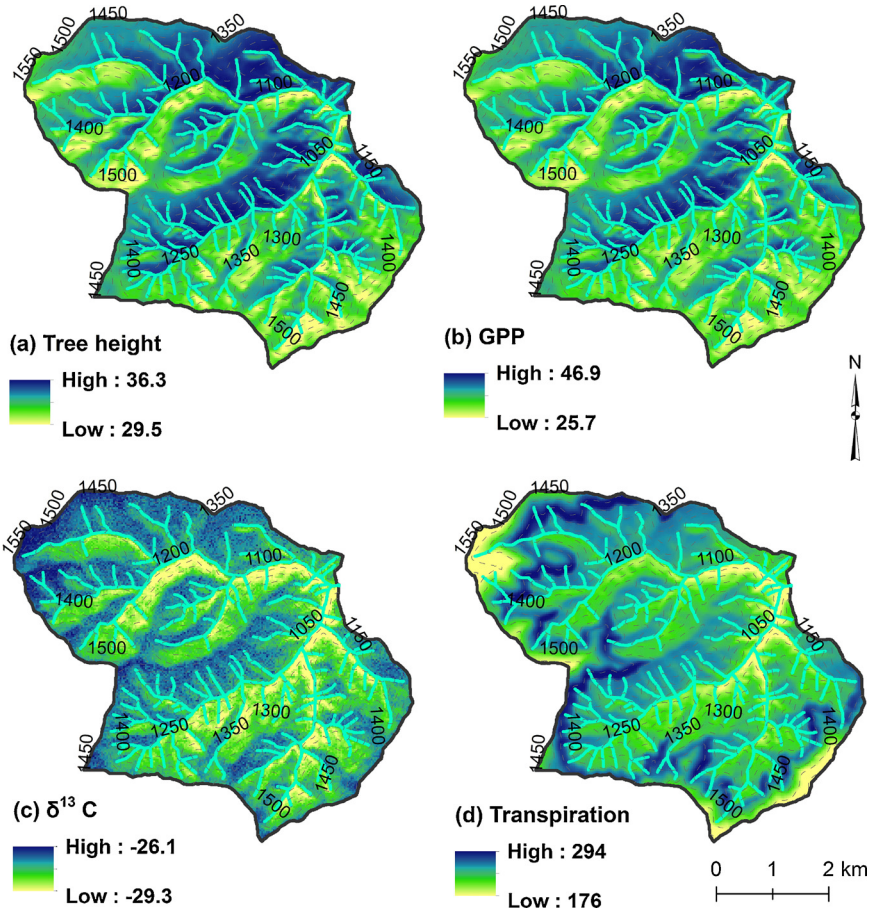

Fig. 8. Model simulated tree height (m), GPP (Mg ha^{-1} $year^{-1}$) (mm $year^{-1}$), tree ring $\delta^{13}C$ (‰), and transpiration (mm $year^{-1}$) of 30 × 30 m grids in 2006. Data shown are simulations of the "Soil Moisture" scenario with variable ASW_x with elevation. Cyan lines show creeks; dashed gray lines show elevation contours with black numbers marked in meters above sea level.

P < 0.01; Fig. 6c). The slope of the increase was 0.00148, 0.00139, and 0.00189‰ m^{-1} (R^2 0.80, 0.80, and 0.89) for the Reference, No Hillshade, and Soil Moisture scenarios respectively, which translated to a ~1‰ (0.96, 0.90, and 1.23‰ respectively) increase in the ~650 m elevational range of MCEW (see Notes S7 and Fig. S12 for additional sensitivity test for $\delta^{13}C$ simulations).

Model simulations predicted variation in tree height, GPP, tree ring $\delta^{13}C$, and transpiration in different aspects across elevations in the Main area. Here we take the most realistic Soil Moisture scenario as the example (Fig. 8 and 9). Simulated tree height, GPP, tree ring $\delta^{13}C$, and transpiration differed among aspects; the values were significantly different with south > east > west > north (ANOVA and Fisher's LSD, P < 0.01). In general, simulated tree height and GPP increased with increasing elevation below ~1150-1250 m and then decreased from ~1250-1600 m. Simulated $\delta^{13}C$ increased with elevation on all aspects (Fig. 9c). Simulated values in 2006 were within a reasonable range compared to available $\delta^{13}C$ measurements of 2006 rings at three sites in MCEW (Fig. 9c). Simulated transpiration at all four aspects peaked at 1380 m (Fig. 9d), matching the elevational peak of VPD and T. We also simulated water use efficiency (WUE) for the whole watershed, which are included in the supporting material (Fig. S14).

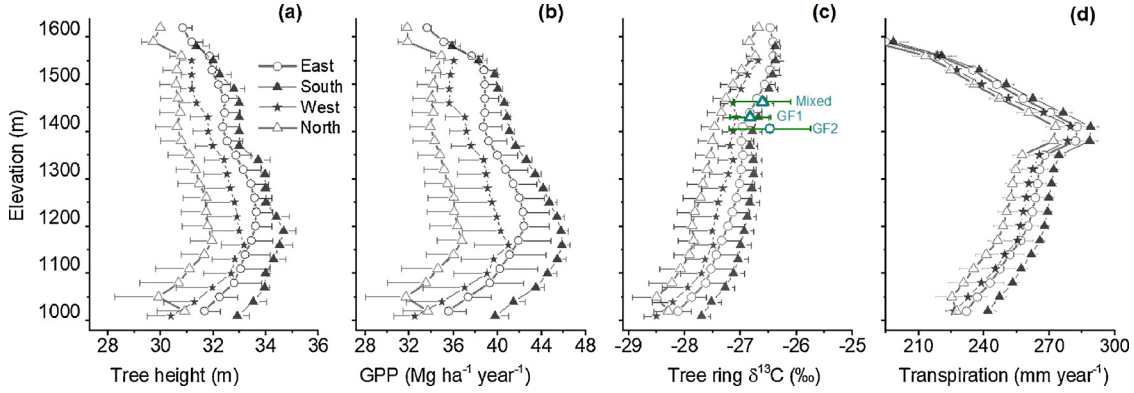

Fig. 9. Simulated elevational variations of tree height, GPP, tree ring $\delta^{13}C$, and transpiration in the MCEW. Data were binned for 30 m elevational bands. The simulations were based on the Soil Moisture scenario with decreasing ASW_x with increasing elevation. Different symbols show the four aspects. Labeled data points in Fig. c show observed $\delta^{13}C$ of tree rings formed in 2006, which were sampled at three sites of Wei et al. (2014a) (labels show locations as in Fig. 1; N = 3 trees at each site). Error bars show standard deviations; one-side standard deviations are shown for simulations for clarity in figures.

4. Discussion

4.1. Temperature inversions

Temperature inversions occurred so frequently (Fig. 4, and S7) that cold valley bottoms can be considered the normal state (Figs. 3 and 4, and S8). They occurred on more than 60% of the days in 2005 and 2006, and on more than 76% of days during the growing season (May-October). On inversion days, the cold-air pool took hours to disperse; as a result, the lower elevations were typically warmer than higher elevations for less than one-third of the diurnal hours and half the daylight hours (e.g. Fig. S8). We found that the upper boundary of the cold-air pool was relatively constant during the inversion days, around ~1370 m, which created two temperature gradients with elevation. Such strong temperature inversions facilitated a unique exploration of whether microclimate or soil moisture more likely determined forest productivity.

4.2. Impacts on forest productivity

Despite dramatic elevational variations in temperature and VPD (Fig. 3 and 4, and S7), the impacts of T and VPD on forest growth in MCEW almost completely offset each other through elevations above 1100 m (the No Hillshade scenario, Fig. 6). This is partly because temperature drives VPD; when temperature was low (reducing GPP), VPD was also low (increasing GPP). But it also because of the sensitivity of photosynthetic gas-exchange to these variables, which is described by the parameterization of the model. The combined climatic impacts are represented by the Reference scenario (realistic climate data, but identical ASW_x), where simulated tree height and GPP increased slightly (~1 m and ~4 Mg ha^{-1} year^{-1} respectively) as elevation increased from ~1000 to ~1150 m and remained relatively constant from ~1150 m upward. Therefore, there was little impact of combined climatic factors on the elevational trend of forest productivity in MCEW. Thus, if we had looked only at the elevational variations of temperature and simulated productivity in the Reference scenarios, we would have concluded that there is no correlation between temperature and productivity in MCEW. This result matches the previous findings that climate is not a strong predictor of productivity, which were estimated at the global scale (Chapin, 2003; Enquist et al., 2007; Kerkhoff et al., 2005; Michaletz et al., 2014). Likewise, in a study across elevations in a tropical montane region (Malhi et al., 2017), temperature also had little impact on either canopy photosynthesis or forest productivity across elevations.

The direct temperature effects in the 3-PG model are to limit photosynthesis in two ways. First, they reduce photosynthesis in non-optimum temperature (see Eqn. A2 in supplementary material) and second, they shut down photosynthesis completely after a frosty night (i.e. frost impact, see Eqn. A3&A4 in supplementary material) (Landsberg and Waring, 1997). In real plants, temperature has other clear effects on photosynthesis (Way and Oren, 2010). Separate from the question of photosynthesis, the process of cell division, which controls growth given sufficient photosynthate, is also tied to temperature (Körner, 1998). Although this issue has primarily been discussed in relation to treeline formation (Körner, 2012; Marshall, 2014), it would likewise influence productivity, if only by limiting the length of the growing season. However, these latter two effects are not built into the model. The model also does not consider plants' local adaptation of plants to thermal and edaphic environment (Enquist et al., 2007; Kerkhoff et al., 2005) which should damp plants' temperature responses. With identical species and physiological parameters across elevations in our simulation, we specifically tested the response of forest productivity to climatic factors. The results indicated that it is the canceling of the direct impacts of temperature and VPD that led to the insensitivity of forest productivity to temperature for this small watershed. We hence urge that future studies should also consider the accompanying VPD impacts when estimating temperature impacts on productivity. These impacts may be especially strong in the riparian zone, where abundant surface water can evaporate and humidify the canopy atmosphere.

If forest productivity was only marginally influenced by the combined effects of temperature and VPD, then the observed elevational trend of H_x was best explained by variation in soil moisture. The best match of observations to simulations was from the most realistic Soil Moisture scenario, which assumed decreasing ASW_x with increasing elevation. The soil is generally thin at ridgetops and deeper in valley floors than on ridges (Bolstad et al., 2001; Helvey et al., 1972; Lin et al., 2006; Markesteijn et al., 2010; Yeakley et al., 1998). The soils mapped in this area at the highest elevations are shallow and rocky. Moreover, ASW_x at valley floors may also be supplemented by converging water flows, including subsurface macropore flow, subsurface lateral flow at the A–B horizon interface, return flow on footslopes and toeslopes, and flow at the soil–bedrock interface (Lin et al., 2006). Forest growth may therefore benefit from more available soil water at low elevations but restrict growth at higher elevations in MCEW. This may also explain why tall canopy trees (> 35 m) in the 1930s-clearcut area occurred more frequently in the Riparian area (Fig. 1), where water was likely more abundant than in the Main area. It would also explain why the lowest tree heights (< 15 m) in the 1930s-clearcut area often occurred at the ridge top (Fig. 1). A previous study indicated a similar elevational trend of forest productivity to our study, with a decrease of aboveground NPP with increasing elevation and hence decreasing soil moisture in Appalachian deciduous forests (Bolstad et al., 2001). On the other hand, temperature also decreases with increasing elevation across the Appalachian sites (Bolstad et al., 2001), confounding temperature and moisture effects. At our site, the frequent inversions broke the covariation between temperature and soil moisture across elevations in this study, which revealed the key role of soil moisture on forest productivity.

The impact of soil moisture on forest productivity may also help to explain the differences between observed H_x and simulated tree height and GPP across aspects. The model predicted tree height and GPP where south- > east- > west- > north- facing slopes (Fig. 9a), consistent with the model's dependence on the amount of solar radiation (Fig. S1). In contrast, observed H_x was similar on east-, north-, and south- facing slopes, but lower on west-facing slopes (Fig. 5b). Depth variations in the nutrient-rich and water-retaining volcanic ash mantles (VAM) may explain these differences. North-facing slopes, especially at higher elevations, generally have significantly deeper VAM (> 32 cm) than more south-westerly facing slopes (~30 cm) in north-central Idaho (Kimsey et al., 2007). Furthermore, ash mantles tend to be shallower (23–33 cm) in the Marblecreek Series soils, which tend to be located on south-facing slopes, relative to the deeper (36–51 cm) mantles in the Bouldercreek Series, which are more common on north-facing slopes (Weisel, 2002). The simulations of forest productivity would likely have had similar aspect patterns to those of H_x if these two factors had been considered, where growth on northerly aspects would be enhanced and on southwesterly aspects would be reduced.

4.3. $\delta^{13}C$ isoscape

The $\delta^{13}C$ simulation provided a rigorous test of the modeled gas exchange predictions. The simulation of $\delta^{13}C$ relies on simulated GPP and simulated canopy conductance (g_c). The simulations for GPP and g_c had to be reasonable before reasonable $\delta^{13}C$ simulations could be reached (Wei et al., 2014a; Wei et al., 2014b). The model predicted a variation of tree ring $\delta^{13}C$ from ~-28.0 to -26.4‰. This was comparable to the observed $\delta^{13}C$ in MCEW (-26.7‰ ± 0.5SD in year 2006 based on 12 trees at four sites from 1299 to 1460 m; see Notes S2).

Our model revealed the variations of $\delta^{13}C$ in the watershed (Fig. 6) and generated $\delta^{13}C$ distribution maps (i.e., isoscapes; Fig. 8c). The modeled elevational change (Fig. 6c; 0.00139–0.00189 ‰ m^{-1}) was

comparable to the observed values of conifer species in Idaho (e.g. 0.0009–0.00268 ‰ m^{-1} for four conifer species in the northern Rocky Mountains, Hultine and Marshall (2000); 0.00105‰ m^{-1} for evergreen species in the northern Rockies, Marshall and Zhang (1994); and for a global database 0.0011‰ m^{-1} Körner et al. (1991)). The similarity in elevation response of predictions vs. observations in this key variable suggests that the gas-exchange parameters were correctly described across the elevation transects. We find this agreement especially compelling because the model was never intended to be tested in this way.

5. Conclusions

This study considered the productivity consequences of elevational heterogeneity of air temperature and VPD in a small watershed. Temperature inversions occurred on 76% of days during the growing season from May to October. The upper boundary of the inversion pool was relatively constant around 1370 m a.s.l. Elevational variations in air temperatures and VPD each had dramatic impacts on the elevational variations in GPP based on model simulations, but their impacts almost completely offset. The observed elevational variation in tree height and GPP was therefore attributed to variation in ASW_x. Observed canopy heights generally decreased with elevation and were lowest on west-facing slopes, consistent with documented variation in soil properties. Simulated elevational trends of simulated tree heights matched those of observations only when realistic elevational variations in ASW_x were used. These results emphasize the importance of quantifying the soil environment when predicting forest productivity in complex terrain.

Acknowledgments

We thank Potlatch Corporation for designing and implementing MCEW and allowing this research to be conducted at MCEW. This work was funded in part by the National Science Foundation EPSCoR - Research Infrastructure Improvement Grant (EPS–0447689), USDA-CSREES NRI grants (2003-35102-13675 and 2006-35102-17689), USFS Research Joint Venture Agreements (#03-JV-11222065-068 and #04-D6-11010000-037). Liang Wei was partially funded by Los Alamos National Laboratory Directed Research & Development (LDRD) program, and John Marshall was supported by the Knut and Alice Wallenberg Foundation (#2015.0047). Special thanks to Terry Cundy at Potlatch Corporation for providing information about MCEW, John Gravelle for maintaining the meteorological stations and resulting dataset, and Chi-Shuang Wang for making Fig. S3. Liang Wei thanks Nate McDowell, Chonggang Xu, Jianwei Zhang, and Bill Elliot for their support. This submission is under public release with the approved LA-UR-17-20232.

Appendix A. Supplementary data

Supplementary material related to this article can be found, in the online version, at doi:https://doi.org/10.1016/j.agrformet.2018.05.012.

References

Adams, E.C., 1979. Cold air drainage and length of growing season in the Hopi Mesas area. Kiva 44 (4), 285–296.
Almeida, A.C., et al., 2010. Mapping the effect of spatial and temporal variation in climate and soils on Eucalyptus plantation production with 3-PG, a process-based growth model. For. Ecol. Manage. 259 (9), 1730–1740.
Ashcroft, M.B., Gollan, J.R., 2012. Fine-resolution (25 m) topoclimatic grids of near-surface (5 cm) extreme temperatures and humidities across various habitats in a large (200 × 300 km) and diverse region. Int. J. Climatol. 32 (14), 2134–2148.
Barry, R.G., 1992. Mountain climatology and past and potential future climatic changes in mountain regions: a review. Mt. Res. Dev. 71–86.
Bigg, G.R., et al., 2014. Synoptic climatology of cold air drainage in the Derwent Valley, Peak District, UK. Meteorol. Appl. 21 (2), 161–170.
Bolstad, P.V., Vose, J.M., McNulty, S.G., 2001. Forest productivity, leaf area, and terrain in southern Appalachian Deciduous forests. For. Sci. 47 (3), 419–427.
Campioli, M., et al., 2015. Biomass production efficiency controlled by management in temperate and boreal ecosystems. Nat. Geosci. 8, 843–846 advance online publication.
Chapin III, F.S., 2003. Effects of plant traits on ecosystem and regional processes: a conceptual framework for predicting the consequences of global change. Ann. Bot. 91 (4), 455–463.
Cleveland, W.S., Grosse, E., Shyu, W.M., 1992. Local regression models. Stat. Models S 309–376.
Coops, N., Waring, R., 2011. A process-based approach to estimate lodgepole pine (&i& Pinus contorta&/i& Dougl.) distribution in the Pacific Northwest under climate change. Clim. Change 105 (1), 313–328.
Coops, N.C., Waring, R.H., 2001. Assessing forest growth across southwestern Oregon under a range of current and future global change scenarios using a process model, 3-PG. Global Change Biol. 7 (1), 15–29.
Daly, C., Conklin, D.R., Unsworth, M.H., 2010. Local atmospheric decoupling in complex topography alters climate change impacts. Int. J. Climatol. 30 (12), 1857–1864.
DeLucia, E.H., Drake, J.E., Thomas, R.B., Gnzalez-Meler, M., 2007. Forest carbon use efficiency: is respiration a constant fraction of gross primary production? Global Change Biol. 13 (6), 1157–1167.
Du, E., Link, T.E., Gravelle, J.A., Hubbart, J.A., 2014. Validation and sensitivity test of the distributed hydrology soil-vegetation model (DHSVM) in a forested mountain watershed. Hydrol. Process. 28 (26), 6196–6210.
Du, E., Link, T.E., Wei, L., Marshall, J.D., 2016. Evaluating hydrologic effects of spatial and temporal patterns of forest canopy change using numerical modelling. Hydrol. Process. 30 (2), 217–231.
Duursma, R., Marshall, J., Robinson, A., Pangle, R., 2007. Description and test of a simple process-based model of forest growth for mixed-species stands. Ecol. Model. 203 (3), 297–311.
Duursma, R.A., Marshall, J.D., Robinson, A.P., 2003. Leaf area index inferred from solar beam transmission in mixed conifer forests on complex terrain. Agric. Forest Meteorol. 118 (3–4), 221–236.
Elliott, K.J., Miniat, C.F., Pederson, N., Laseter, S.H., 2015. Forest tree growth response to hydroclimate variability in the southern Appalachians. Global Chang Biol. 21 (12), 4627–4641.
Enquist, B.J., Kerkhoff, A.J., Huxman, T.E., Economo, E.P., 2007. Adaptive differences in plant physiology and ecosystem paradoxes: insights from metabolic scaling theory. Global Change Biol. 13 (3), 591–609.
Farquhar, G.D., Ehleringer, J.R., Hubick, K.T., 1989. Carbon isotope discrimination and photosynthesis. Annu. Rev. Plant Biol. 40 (1), 503–537.
Fleagle, R.G., 1950a. Radiation theory of local temperature differences. J. Meteorol. 7 (2), 114–120.
Fleagle, R.G., 1950b. A theory of air drainage. J. Meteorol. 7 (3), 227–232.
Galmés, J., Flexas, J., Savé, R., Medrano, H., 2007. Water relations and stomatal characteristics of Mediterranean plants with different growth forms and leaf habits: responses to water stress and recovery. Plant Soil 290 (1), 139–155.
Gessler, P.E., Chadwick, O.A., Chamran, F., Althouse, L., Holmes, K., 2000. Modeling soil–landscape and ecosystem properties using terrain attributes. Soil Sci. Soc. Am. J. 64 (6), 2046–2056.
Gessler, P.E., Moore, I.D., McKenzie, N.J., Ryan, P.J., 1995. Soil-landscape modelling and spatial prediction of soil attributes. Int. J. Geogr. Inf. Syst. 9 (4), 421–432.
Goulden, M.L., Miller, S.D., da Rocha, H.R., 2006. Nocturnal cold air drainage and pooling in a tropical forest. J. Geophys. Res. 111 D08S.
Goulden, M.L., et al., 2011. Patterns of NPP, GPP, respiration, and NEP during boreal forest succession. Glob. Change Biol. 17 (2), 855–871.
Helvey, J.D., Hewlett, J.D., Douglass, J.E., 1972. Predicting soil moisture in the Southern Appalachians. Soil Sci. Soc. Am. J. 36 (6), 954–959.
Holden, Z.A., Abatzoglou, J.T., Luce, C.H., Baggett, L.S., 2011a. Empirical downscaling of daily minimum air temperature at very fine resolutions in complex terrain. Agric. For. Meteorol. 151 (8), 1066–1073.
Holden, Z.A., Crimmins, M.A., Cushman, S.A., Littell, J.S., 2011b. Empirical modeling of spatial and temporal variation in warm season nocturnal air temperatures in two North Idaho mountain ranges, USA. Agric. Forest Meteorol. 151 (3), 261–269.
Hubbart, J., Link, T., Campbell, C., Cobos, D., 2005. Evaluation of a low-cost temperature measurement system for environmental applications. Hydrol. Process. 19 (7), 1517–1523.
Hubbart, J.A., Kavanagh, K.L., Pangle, R., Link, T., Schotzko, A., 2007a. Cold air drainage and modeled nocturnal leaf water potential in complex forested terrain. Tree Physiol. 27 (4), 631–639.
Hubbart, J.A., Link, T.E., Gravelle, J.A., 2015. Forest canopy reduction and snowpack dynamics in a Northern Idaho watershed of the Continental-Maritime region, United States. For. Sci. 61 (5), 882–894.
Hubbart, J.A., Link, T.E., Gravelle, J.A., Elliot, W.J., 2007b. Timber harvest impacts on water yield in the Continental/Maritime hydroclimatic region of the United States. For. Sci. 53 (2), 169–180.
Hudak, A.T., et al., 2006. Regression modeling and mapping of coniferous forest basal area and tree density from discrete-return lidar and multispectral satellite data. Can. J. Remote Sens. 32 (2), 126–138.
Hudak, A.T., Crookston, N.L., Evans, J.S., Hall, D.E., Falkowski, M.J., 2008. Nearest neighbor imputation of species-level, plot-scale forest structure attributes from LiDAR data. Remote Sens. Environ. 112 (5), 2232–2245.
Hultine, R.K., Marshall, D.J., 2000. Altitude trends in conifer leaf morphology and stable carbon isotope composition. Oecologia 123 (1), 32–40.
Jensen, J.L.R., Humes, K.S., Vierling, L.A., Hudak, A.T., 2008. Discrete return lidar-based prediction of leaf area index in two conifer forests. Remote Sens. Environ. 112 (10), 3947–3957.
Johnson, D.M., et al., 2018. Co-occurring woody species have diverse hydraulic strategies

and mortality rates during an extreme drought. Plant Cell Environ. 41 (3), 576–588.
Keppel, G., et al., 2012. Refugia: identifying and understanding safe havens for biodiversity under climate change. Global Ecol. Biogeogr. 21 (4), 393–404.
Kerkhoff, A.J., Enquist, B.J., Elser, J.J., Fagan, W.F., 2005. Plant allometry, stoichiometry and the temperature-dependence of primary productivity. Global Ecol. Biogeogr. 14 (6), 585–598.
Kimsey, M., Gardner, B., Busacca, A., 2007. Ecological and topographic features of volcanic ash-influenced forest soils. In: Page-Dumroese, D., Miller, R., Mital, J., McDaniel, P., Miller, D. (Eds.), Volcanic-Ash-Derived Forest Soils of the Inland Northwest: Properties and Implications for Management and Restoration. U.S. Department of Agriculture, Forest Service, Rocky Mountain Research Station, Fort Collins, CO, pp. 7–21.
Körner, C., 1998. A re-assessment of high elevation treeline positions and their explanation. Oecologia 115 (4), 445–459.
Körner, C., 2012. Alpine Treelines: Functional Ecology of the Global High Elevation Tree Limits. Springer Science & Business Media.
Körner, C., Farquhar, G., Wong, S., 1991. Carbon isotope discrimination by plants follows latitudinal and altitudinal trends. Oecologia 88 (1), 30–40.
Kräuchi, N., Brang, P., Schönenberger, W., 2000. Forests of mountainous regions: gaps in knowledge and research needs. For. Ecol. Manage. 132 (1), 73–82.
Landsberg, J.J., Waring, R.H., 1997. A generalised model of forest productivity using simplified concepts of radiation-use efficiency, carbon balance and partitioning. For. Ecol. Manage. 95 (3), 209–228.
Lin, H., Kogelmann, W., Walker, C., Bruns, M., 2006. Soil moisture patterns in a forested catchment: a hydropedological perspective. Geoderma 131 (3), 345–368.
Litton, C.M., Raich, J.W., Ryan, M.G., 2007. Carbon allocation in forest ecosystems. Glob. Change Biol. 13 (10), 2089–2109.
Lundquist, J.D., Pepin, N., Rochford, C., 2008. Automated algorithm for mapping regions of cold-air pooling in complex terrain. J. Geophys. Res. 113 (D22), D22107.
Malhi, Y., et al., 2017. The variation of productivity and its allocation along a tropical elevation gradient: a whole carbon budget perspective. New. Phytol. 214, 1019–1032.
Manins, P.C., Sawford, B.L., 1979. Katabatic winds: a field case study. Q. J. R. Meteorol. Soc. 105 (446), 1011–1025.
Markesteijn, L., Iraipi, J., Bongers, F., Poorter, L., 2010. Seasonal variation in soil and plant water potentials in a Bolivian tropical moist and dry forest. J. Trop. Ecol. 26 (05), 497–508.
Marshall, J.D., 2014. CO2 enrichment at treeline: help or hindrance for trees on the edge? Plant, Cell Environ. 37 (2), 312–314.
Marshall, J.D., Zhang, J., 1994. Carbon isotope discrimination and water-use efficiency in native plants of the north-central Rockies. Ecology 1887–1895.
Michaletz, S.T., Cheng, D., Kerkhoff, A.J., Enquist, B.J., 2014. Convergence of terrestrial plant production across global climate gradients. Nature 512, 39–43.
Minder, J.R., Mote, P.W., Lundquist, J.D., 2010. Surface temperature lapse rates over complex terrain: lessons from the Cascade mountains. J. Geophys. Res. 115 (D14), D14122.
Moore, I.D., Gessler, P.E., Nielsen, G.A., Peterson, G.A., 1993. Soil attribute prediction using terrain analysis. Soil Sci. Soc. Am. J. 57 (2), 443–452.
Nippert, J.B., Marshall, J.D., 2003. Sources of variation in ecophysiological parameters in Douglas-fir and grand fir canopies. Tree Physiol. 23 (9), 591–601.
Novick, K., Brantley, S., Miniat, C.F., Walker, J., Vose, J.M., 2014. Inferring the contribution of advection to total ecosystem scalar fluxes over a tall forest in complex terrain. Agric. Forest Meteorol. 185, 1–13.
Novick, K.A., Oishi, A.C., Miniat, C.F., 2016. Cold air drainage flows subsidize montane valley ecosystem productivity. Glob Chang Biol 22 (12), 4014–4027.
Oyler, J.W., Dobrowski, S.Z., Ballantyne, A.P., Klene, A.E., Running, S.W., 2015. Artificial amplification of warming trends across the mountains of the western United States. Geophys. Res. Lett. 42 (1), 153–161.
Schimel, D., et al., 2002. Carbon sequestration studied in western U.S. mountains. Eos Trans. Am. Geophys. Union 83 (40), 445–449.
Suggitt, A.J., et al., 2011. Habitat microclimates drive fine-scale variation in extreme temperatures. Oikos 120 (1), 1–8.
Vicca, S., et al., 2012. Fertile forests produce biomass more efficiently. Ecol. Lett. 15 (6), 520–526.
Wallace, J.M., Hobbs, P.V., 2006. Atmospheric Science: An Introductory Survey, 92. Academic press.
Waring, R.H., Landsberg, J.J., Williams, M., 1998. Net primary production of forests: a constant fraction of gross primary production? Tree Physiol. 18 (2), 129–134.
Way, D.A., Oren, R., 2010. Differential responses to changes in growth temperature between trees from different functional groups and biomes: a review and synthesis of data. Tree Physiology. tpq015.
Wei, L., Marshall, J., Zhang, J., 2008. Quantum yields in mixed-conifer forests and Ponderosa Pine plantations. AGU Fall Meet 1, 0350. http://dx.doi.org/10.13140/RG.2.2.22839.52645. Abstracts.
Wei, L., et al., 2014a. Constraining 3-PG with a new $\delta^{13}C$ submodel: a test using the δ13C of tree rings. Plant Cell Environ. 37 (1), 82–100.
Wei, L., Marshall, J.D., Zhang, J., Zhou, H., Powers, R.F., 2014b. 3-PG simulations of young ponderosa pine plantations under varied management intensity: why do they grow so differently? For. Ecol. Manage. 313 (0), 69–82.
Weisel, C.J., 2002. In: N.R.c. United States Department of Agriculture (Ed.), Soil Survey of St. Joe Area, Parts of Benewah and Shoshone Counties, Idaho.
Weiskittel, A.R., Crookston, N.L., Radtke, P.J., 2011. Linking climate, gross primary productivity, and site index across forests of the western United States. Can. J. For. Res. 41 (8), 1710–1721.
Whiteman, C.D., 2000. Mountain Meteorology: Fundamentals and Applications. Oxford University Press 355 pp.
Wykoff, W.R., Crookston, N.L., Stage, A.R., 1982. User's Guide to the Stand Prognosis Model. General Technical Report. INT-133. USDA Forest Service, Intermountain Forest and Range Experiment Station.
Yeakley, J., Swank, W., Swift, L., Hornberger, G., Shugart, H., 1998. Soil moisture gradients and controls on a southern Appalachian hillslope from drought through recharge. Hydrol. Earth Syst. Sci. Discuss. 2 (1), 41–49.
Yi, C., 2008. Momentum transfer within canopies. J. Appl. Meteorol. Climatol. 47 (1), 262–275.